Environmental Modelling and Software 108 (2018) 91–101

Contents lists available at ScienceDirect

Environmental Modelling & Software

journal homepage: www.elsevier.com/locate/envsoft

Evaluation of *E.coli* losses in a tidal river network using a refined 1-D numerical model

Guoxian Huang[a,b], Roger A. Falconer[a,*], Binliang Lin[a,c]

[a] Hydro-environmental Research Centre, School of Engineering, Cardiff University, Cardiff CF10 3XQ, UK
[b] State Key Laboratory of Plateau Ecology and Agriculture, Qinghai University, Xining 810016, China
[c] Department of Hydraulic Engineering, Tsinghua University, Beijing, 100084, China

ARTICLE INFO

Keywords:
Mass transport
One-dimensional model
River networks
Multiple stagnations
E.coli loss

ABSTRACT

Predicting the rate of *Escherischia coli (E.coli)* loss in a river network is one of the key conditions required in the management of bathing waters, with well verified numerical models being effective tools used to predict bathing water quality in regions with limited field data. In this study, a unique finite volume method (FVM) one-dimensional model is firstly developed to solve the mass transport process in river networks, with multiple moving stagnation points. The model is then applied to predict the concentration distribution of *E.coli* in the river Ribble network, UK, where the phenomena of multiple stagnation points and different flow directions appear extensively in a tidal sub-channel network. Validation of the model demonstrates that the proposed method gives reasonably accurate solution. The verification results show that the model predictions generally agree well with measured discharges, water levels and *E.coli* concentration values, with mass conservation of the solution reaching 99.0% within 12 days for the Ribble case. An analysis of 16 one-year scenario runs for the Ribble network shows that the main reduction in *E.coli* concentrations occurs in the riverine and estuarine regions due to the relatively large decay rate in the brackish riverine waters and the long retention time, due to the complex river discharge patterns and the tidal flows in the regions.

1. Introduction

Escherischia coli (E.coli) loss at the river-estuary transition zone is a complex process where decay and production through various sources coexist. The pattern of *E.coli* loss varies from case to case, and is governed by their biotic intrinsic parameters, abiotic environmental conditions and episodic sources. Field sampled data are important in the evaluation of the fate of *E.coli*, but they are usually limited. Therefore, numerical models are often used, together with limited field measurements and laboratory analysis to evaluate quantitatively the *E.coli* losses in riverine and coastal waters (Servais et al., 2007). However, the accuracy of the models used needs to be verified to ensure that the solutions are stable and mass conservative, as well as including appropriate values for key parameters such as: bed roughness, dispersion and decay rates (Steets and Holden, 2003).

A mass conserved, stable, accurate and computationally manageable model is therefore a prerequisite for *E.coli* concentration evaluation, since rainfall-runoff intensities enter river channels in pulses, often at minute scales, creating large gradients in pollutant concentrations (Sanders et al., 2001). This is especially important in complex river networks with relatively steep gradients and also where highly unsteady tidal currents exist in the estuarine and coastal zones. A small mass-conservation error in the hydrodynamic solution may cause a large error in the matter transport solution (Bousso et al., 2012). However, it is often difficult to obtain highly conservative solutions in a natural river system for a number of reasons, including: the use of non-consistent governing equations (Aral et al., 2000), partial or full linearization of the governing equations, different discretized formats between the hydrodynamic and mass transport model equations etc. In order to improve on the mass conservation properties of such solutions, the finite volume method (FVM) (Murillo and Navas-Montilla, 2016; Wu and Wang, 2008; Zhang et al., 2011) is increasingly used in water quality modelling studies, together with an unstructured grid. However, when an explicit FVM model is used, two key shortcomings remain, one being the smaller time step imposed by the Courant-Friedrichs-Lewy (CFL) limiting condition (Delis et al., 2000; Stelling, 2003), and the difficulty in maintaining robustness for complex looped and dendritic river networks (Jin et al., 2002). For long-term simulations, e.g. for up to 100 years, and for a series of scenario runs of the hydrodynamic, sediment and mass transport processes, 1D models are extensively used

* Corresponding author.
E-mail address: FalconerRA@cardiff.ac.uk (R.A. Falconer).

https://doi.org/10.1016/j.envsoft.2018.07.009
Received 9 July 2017; Received in revised form 18 February 2018; Accepted 19 July 2018
Available online 23 July 2018

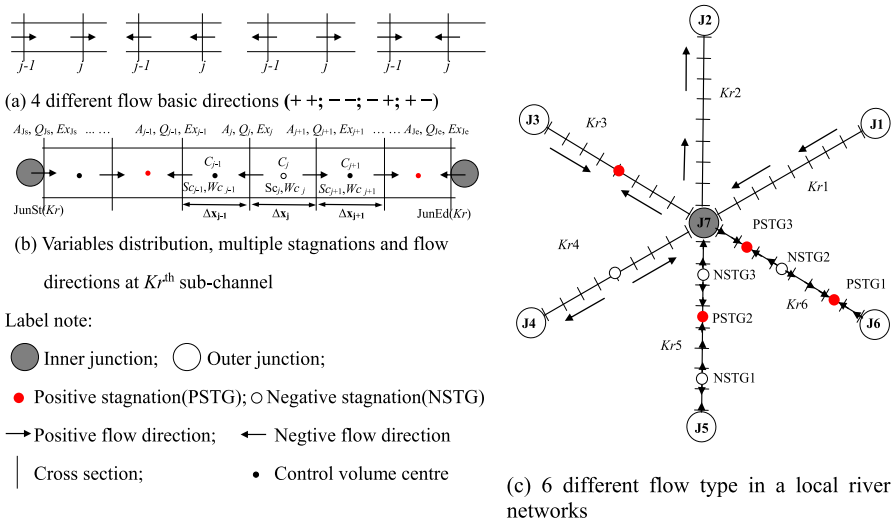

Fig. 1. Four flow directions and multiple stagnation points and positions for key variables.

because of their higher efficiency and even higher accuracy than 2D and 3D models when dealing with large and complex river networks (Lauer et al., 2016; Wu et al., 2004; Zhou and Lin, 1998). Usually a 1-D model is used to link a catchment hydrological model (Merkhali et al., 2015; Paiva et al., 2011) and a 2D or 3D estuarine and/or coastal model (Bladé et al., 2012; Twigt et al., 2009). Therefore, 1D models are generally invaluable tools in an integrated modelling system for simulating hydrological, hydrodynamic and mass transport processes, from the catchment cells to river networks, and then to the receiving estuarine and coastal waters (Nanía et al., 2014; Salvadore et al., 2015).

In general different flow directions often exist in estuaries caused by the river flow and tidal waves and there four basic flow directions can exist in a sub-channel, including: (i) down flow, (ii) up flow, (iii) inward-flow, and (iv) outward-flow (Zhang et al., 2014). For the case of (iii), or (iv), a positive stagnation point, or a negative stagnation point, will occur (see Fig. 1c). However in a sub-channel there may be more than one stagnation point and the number of stagnation points and their locations can change continuously due to the interaction between the tides and river flows. Stagnation can also occur at more than a single point in an estuary and/or river reach. Therefore, an existing algorithm for dealing with only one stagnation, developed by Hu et al. (2010) and Zhang et al. (2014), has been refined in the current study to enable the physical processes of multiple stagnation zones to be predicted.

The main objective of this study is therefore to improve on the accuracy of numerical model predictions of *E.coli* losses in river networks and to reduce the error level in mass conservation. Details are given of the development of a FVM based model to simulate the mass transport processes in river and estuarine networks, particularly where multiple stagnation zones and different flow directions may occur. Firstly, in this model a new algorithm is developed to predict the formation of multiple stagnation zones and the mass transport processes in these zones. Secondly, a dynamic decay rate is formulated for different salinity and radiation levels, based on data obtained from laboratory studies and field investigation. Thirdly, field measured hydrodynamic and *E.coli* data, acquired for the river Ribble network and Fylde coast in 2012, are used to calibrate and validate the hydro-epidemiological model. Finally, the loss of *E.coli* in the river Ribble network is evaluated using the refined 1D model. A series of scenario simulations are also reported, using the refined 1D modelling system, and the *E.coli* losses in the middle and lower regions of the river Ribble, including different sources from 47 sub-catchments, are quantitatively predicted. The results show the importance of the need for model mass conservation, especially in the lower reaches of the river basin, where the reversing current and the multiple stagnation zones appear extensively, driven by tidal and river flow interactions.

2. Theory/model framework

2.1. Hydrodynamic model

The St Venant equations are widely used as the governing equations to predict the hydrodynamic processes in river networks, as given by:

$$B\frac{\partial Z}{\partial t} + \frac{\partial Q}{\partial x} = q \tag{1}$$

$$\frac{\partial Q}{\partial t} + \frac{\partial}{\partial x}\left(\frac{Q^2}{A}\right) + gA\left(\frac{\partial Z}{\partial x} + s_f + s_e\right) + L = 0 \tag{2}$$

where B = wetted-cross sectional width (m), Z = elevation of water surface above datum (m), Q = river discharge (m^3/s), q = lateral discharge per unit channel width (m^2/s), x = curvilinear distance of river channel (m), t = time (s), A = wetted cross sectional area (m^2), g = gravitational acceleration (m/s^2), s_f = friction slope, expressed as $s_f = {}^{n^2 Q|Q|}/_{A(A/B)^{4/3}}$, in which n = Manning's coefficient, s_e = local longitudinal slope of water surface due to localised head losses, and L = momentum of lateral discharge inputs.

2.2. Mass transport model

The mass transport equation given as:

$$\frac{\partial(AC)}{\partial t} + \frac{\partial(QC)}{\partial x} - \frac{\partial}{\partial x}\left(AE_x\frac{\partial C}{\partial x}\right) = S_C + W_C \tag{3}$$

where E_x = longitudinal dispersion coefficient, which is based on a formula derived by Fisher (Fischer, 1973), S_C = a source term due to bacterial decay ($S_C = Ins - K{\cdot}C$), K = decay rate (hr^{-1}), Ins = constant source term, for *E.coli* this term is zero. In engineering studies, the T_{90}, which is the time needed for 90% of the bacteria to die off (T_{90} = ln10/K, unit is hr), is usually used.The value of T_{90} is related to radiation, salinity and organic matter, etc(Yang et al., 2008). The limited measured data is given in Table 1(Huang et al., 2017) based on radiation and salinity condition then intepolated T_{90} is used in the model based on the given radiation and modelled salinity. W_C = external sources from point and diffuse source inputs, which is decided by the *E.coli* flux from lateral sub-catchments.

The FVM is used to improve on the mass conservation of Eq. (3). However, the consistency between Appendix S1: Eqs. (2)–(3) and Eq. (3) may not be entirely satisfactory, because of the additional errors

Table 1
Parameters used in the 1-D model.

Label	Value	Note and reference
Δt	30	Normal time step (Sec)
Δt_1	3	Smaller time step used in limited additional inner iterations (Sec)
Δx	20–100	distance between 2 cross-sections (m)
Nsc	1031	Cross-section number
NRiv	9	Sub-channel number
PS	47	Point source number
T_{90}	6–48	Decay rate (hr)
θ	0.6–1.0	Explicit-implicit coefficient
θ_T	1.013	Temperature coefficient
$\bar{\theta}$	0.1	Return coefficient at lower boundary

introduced by the linearization in deriving Appendix S1: Eqs. (2)–(3). Therefore, a small time step approach is used, i.e., several inner iterations are carried out within a time step to reduce the errors in the solution of the hydrodynamic equations. In this way, the mass conservation level is improved in the solution of Eq. (3). The staggered grids, where the hydrodynamic and water quality variables are located at the cross sections and the centre of a control volume, respectively (see Fig. 1), are used to further reduce the mass conservation error.

After obtaining the solution of concentrations at junctions, an explicit method is used to determine the *E.coli* concentration value for each control volume. For the case of a positive flow, the mass transport equation (Eq. (3)) is discretized using the implicit upwind scheme, as given in Eq. (4):

$$\frac{\partial(AC)}{\partial t} = \frac{(\overline{A}\,C)_j^{k+1} - (\overline{A}\,C)_j^k}{\Delta t} \tag{4a}$$

$$\frac{\partial(QC)}{\partial x} = \frac{(QC)_j^{k+1} - (QC)_{j-1}^{k+1}}{\Delta x_{j-1}} \tag{4b}$$

$$-\frac{\partial}{\partial x}\left(AE_x\frac{\partial C}{\partial x}\right) = \frac{1}{\Delta x_{j-1}}\left[(AE_x)_{j-1}^{k+1}\cdot\frac{C_j^{k+1} - C_{j-1}^{k+1}}{\frac{\Delta x_{j-2}+\Delta x_{j-1}}{2}} - (AE_x)_j^{k+1}\cdot\frac{C_{j+1}^{k+1} - C_j^{k+1}}{\frac{\Delta x_j+\Delta x_{j-1}}{2}}\right] \tag{4c}$$

$$S_C + W_C = (\overline{A}\,\overline{K}C)_j^{k+1} + (Ins + W_C)^{k+1} \tag{4d}$$

Where $\overline{A}_j^k$, $\overline{B}_j^k$, $\overline{Z}_j^k$ = average river area, width and water elevation in the jth control volume, respectively, at the kth time step. The linear equations for the Krth sub-channel can be written as:

$$a_j C_{j-1}^{k+1} + b_j C_j^{k+1} + c_j C_{j+1}^{k+1} = zz_j \cdot (j = Js, Js+1, \cdots, Je) \tag{5}$$

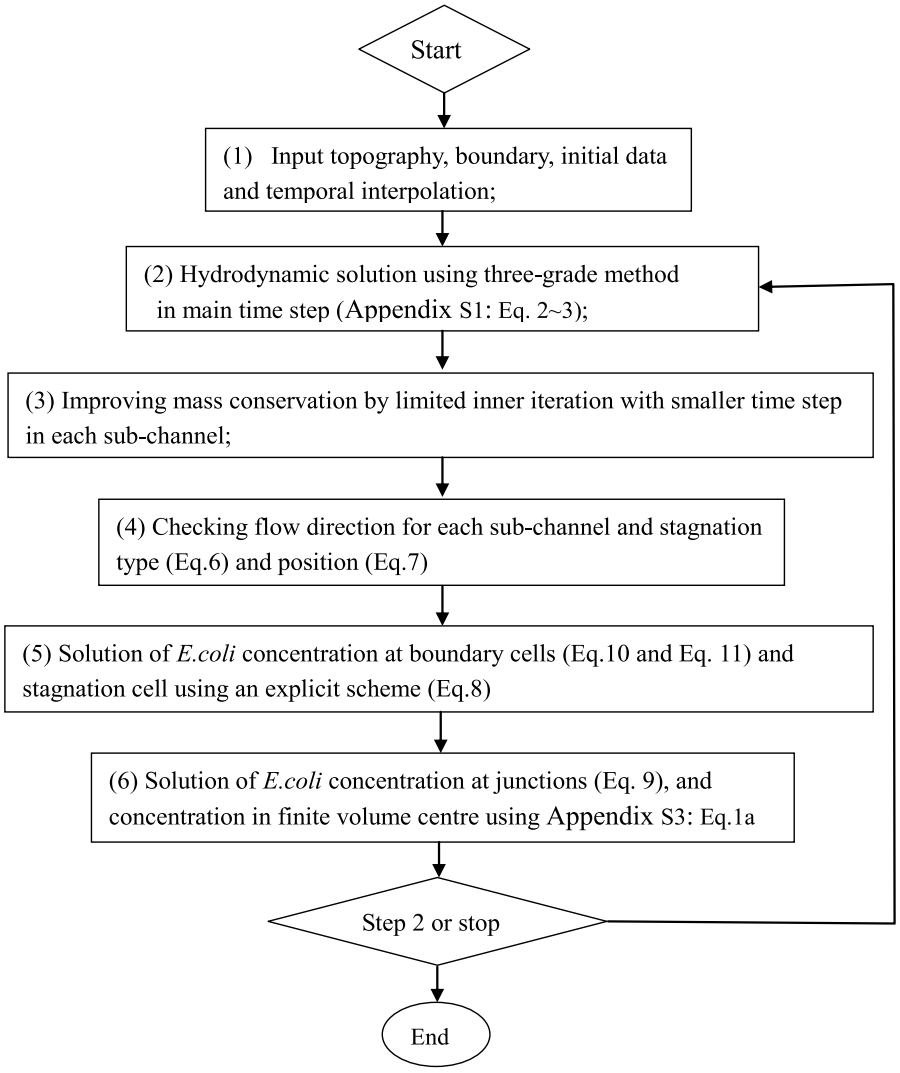

Fig. 2. Main solution procedure of the refined 1-D model.

where $a_j b_j$, c_j = coefficients, zz_j = explicit term, C_j^{k+1} = mass concentration in control volume j at the $k+1$th time step, Js, Je = the start and end cross-section number for the Krth sub-channel, respectively. The other three flow directions types are discretized in a similar manner. For the flow pattern shown in Fig. 1b, the coefficients a_j, b_j, c_j, zz_j in the inner cross-sections (j = Js,Js+1, …,Je) are derived in a similar manner as for the euquations (1) and (2), see Appendix S2: Eq. (1).

In order to predict the flow patterns in tidal river reaches with multiple stagnation points a refined algorithm has been developed based on existing work (Zhang et al., 2014). In this model: (i) a search was carried for each cross section to identify the existence of a stagnation in a sub-channel and possible position using Eq. (6) and Eq. (7); (ii) the flow and stagnation type is identified based on theflow direction distributions (see Kr1¬6 in Fig. 1c) and solute concentrations within the inner junctions, where multiple stagnation points existed, using Eq. (8); and (iii) a set of linear equations and related parameters were reconstructed for a junction with multiple stagnations in the mass transport solution (see Eq. (9)). Once the values of the concentration at the kth time step are known, the concentration values at the $k+1$th time step, for the Krth sub-channel, can then be calculated using Appendix: S3, Eq. (1), together with the concentration values at the starting and ending junctions. Moreover, because the lower *E.coli* concentration boundary is required during a flood tide, the simplified lower boundary is given using Eq. (10) and Eq. (11). Based on the refinement steps above, the main procedure used to solve the hydrodynamic and mass transport equations are shown in a flowchart in Fig. 2.

Identification of a stagnation point in a sub-channel, based on the flow directions at two adjacent cross-sections of a control volume:

$$Q_{j-1} \cdot Q_j < 0 \tag{6}$$

A moving stagnation zone's position ($XSTG$, $YSTG$) is identified by Eq. (7):

$$\begin{cases} XSTG = XT_{j-1} + |Q_{j-1}|/(|Q_{j-1}| + |Q_j|) \cdot (XT_j - XT_{j-1}) \\ YSTG = YT_{j-1} + |Q_{j-1}|/(|Q_{j-1}| + |Q_j|) \cdot (YT_j - YT_{j-1}) \end{cases} \tag{7}$$

where XT_j, YT_j = coordinates at the jth cross section of a sub-channel.

If there are m stagnation points ($m \geq 2$) in a sub-channel, there will be m+1 reaches, with each having a single flow direction (+or −). The *E.coli* concentrations of each control volume can be predicted using the formulae for the "+ +" and "− −" flow patterns if the concentration values for each stagnation zone are given. The *E.coli* concentration for a control volume with a stagnation point is solved for in two steps:

Step 1 Solving the C_j^{k+1} at the control volume with the stagnation

There are two types of stagnations; one is the positive stagnation, where water flows inwards, and the other is the negative stagnation, where water flows outwards. An explicit upwind scheme is used to determine the *E.coli* concentration value at the control volume with a stagnation point. For example, for a positive stagnation case, then C_j^{k+1} is determined using Eq. (8):

$$\begin{aligned} C_j^{k+1} &= \frac{A_{M_j}^{k}}{A_{M_j}^{k+1}} C_j^k - \frac{\Delta t}{A_{M_j}^{k+1}} \frac{Q_{j-1}^{k+1} C_j^k - Q_j^{k+1} C_j^k}{\Delta x_{j-1}} \\ &+ \frac{\Delta t}{\Delta x_{i-1} A_{M_j}^{k+1}} \left[(AE_x)_{i-1}^{k+1} \cdot \frac{C_{i-1}^k - C_i^k}{\frac{\Delta x_{i-2} + \Delta x_{i-1}}{2}} - (AE_x)_i^{k+1} \cdot \frac{C_i^k - C_{i+1}^k}{\frac{\Delta x_i + \Delta x_{i-1}}{2}} \right] \\ &+ \frac{\Delta t}{A_{M_j}^{k+1}} \cdot (S_C + W_C)_j^{k+1} \end{aligned} \tag{8}$$

Step 2 Re-construction of linear systems with multiple stagnations.

Here we use Fig. 1 c to illustrate the construction of the equations for the four flow directions and multiple moving stagnation zones. Assuming that the mass is well mixed at the junction and omitting the junction's storage variation, the mass conservation equation for J7 (see Fig. 1c) can be written as:

$$\begin{aligned} &Q_{Kr1}(Je) \cdot C_{Kr1}(Je) + Q_{Kr4}(Je) \cdot C_{Kr4}(Je) + Q_{Kr5}(Je) \cdot C_{Kr5}(Je) \\ &+ (Q_{Kr2}(Je) + Q_{Kr3}(Je) + Q_{Kr6}(Je)) \cdot C_{J7} = 0 \end{aligned} \tag{9}$$

The parameters of implicit algebraic equations (Eq. (5)) can be solved using Appendix S2: Eqs. (1) and (2). During the construction of the concentration equation at a junction linked with boundaries, the upper concentration boundary value is required for a positive flow or the low concentration boundary value is required only for a negative flow. For a sub-channel with multiple stagnation points, only the concentration values at the first and last negative stagnation points are needed. The number and position of the stagnation point(s) may change, but the matrix structure remains the same. After solving the concentration at the internal junctions using Eq. (9), then the concentration at the control volume centre for every sub-channel can be solved using Appendix S3: Eq. (1).

During a flood tide, a lower boundary condition is required and water elevation and *E.coli* concentration values need to be specified. However, it is often difficult to obtain the measured *E.coli* concentration data. Herein we follow the returned coefficient concept proposed by Falconer (1984) which is expressed in Eq. (10):

$$C(t) = \overline{\theta} \cdot \overline{C} \tag{10}$$

where $C(t)$ = *E.coli* concentration input from the sea boundary at time t; $\overline{\theta}$ = *E.coli* loss coefficient, which ranges from 0.0 to 1.0; $\overline{C}$ = mean *E.coli* concentration across the sea boundary, defined as:

$$\overline{C} = \int_{t_1}^{t_2} Q(t) C(t) dt \Big/ \int_{t_1}^{t_2} Q(t) dt \tag{11}$$

In order to reduce the uncertainty level, a series of the virtual volumes have been added to the seaward boundary to store the outflow and *E.coli* during the ebb tides, and a proportion of the integrated *E.coli* efflux will return to the riverine networks through the sea boundary during the subsequent flood tides. The *E.coli* losses are mainly caused by two mechanisms: one is related to the tidal and river flow characteristics, and the other is by the natural decay of *E.coli* in the virtual volumes.

3. Application

3.1. Model setup for the Ribble case, UK

The Ribble river basin is located in the North West of England. It originates from the rural hills of the Yorkshire Dales and the source of the river Ribble, to major urban areas of Lancashire, including: Blackburn, Burnley and Preston, with an area of 1583 km^2. It has 4 key tributaries, including: the rivers Hodder, Calder, Darwen and Douglas, as well as the Crossens drainage system which flows into the Ribble estuary (see Fig. 3). It is the only UK research catchment for studies linked to the EU Water Framework Directive (WFD) implementation (Kay et al., 2005) and a significant amount of historical data on the river topography, hydrology, water quality and *E.coli* measurements have been collected over the past 20 years.

The following data were used in the model: (i) bathymetric data in the estuary and riverine regions, which were converted into 1-D cross-

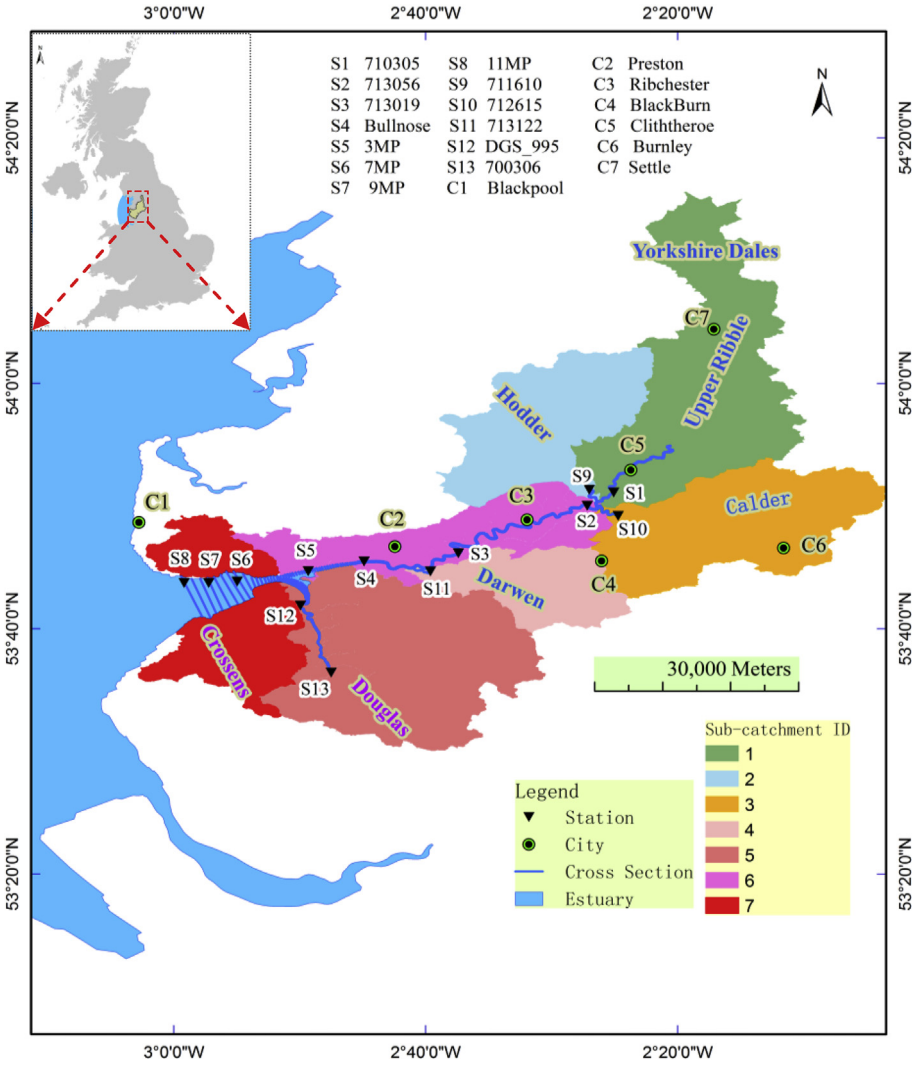

Fig. 3. Model domain of the river Ribble and catchments, showing the 7 sub-domains.

section data by interpolation (Huang et al., 2014); (ii) 15 min sampled discharges and hourly *E.coli* concentration data predicted at 5 main upper river boundaries, namely the Ribble (No.710305), Hodder (No. 711610), Calder (No. 712615), Darwen (No. 713122), and Douglas (No.700306), and 7 sub-catchments, as shown in Fig. 3; (iii) the inflow and *E.coli* boundaries from 5 main upper rivers and 47 minor branches, provided by the UK Environment Agency (EA) and Sheffield University using the Hydrological Simulation Program FORTRAN (HSPF) (Bicknell et al., 1997) and Infoworks (Wallingford Software Ltd, 1995) models; and (iv) half-hour tidal elevation data at the lower boundary. Hourly meteorological data were acquired at 9 stations around the 1-D model domain and interpolated into the cross sections of the 1-D model. These data included air and earth temperatures, radiation levels, relative humidity, rainfall etc., with the data being provided by the British Atmospheric Data Centre, UK (http://badc.nerc.ac.uk/home/). The main parameters used in the model are listed in Table 1.

3.2. Mass conservation test

In order to test the refined model two objective functions were used to check the mass conservation level: (i) temporal difference between the net input flow volume and water storage across the whole model domain (ΔVW_{OBJ}^{k+1}); (ii) accumulated water conservation error ($SumVW_{OBJ}^{k+1}$). They are expressed as:

$$\Delta VW_{OBJ}^{k+1} = VWIO^{k+1} - DVW^{k+1} \tag{12a}$$

$$SumVW_{OBJ}^{k+1} = SumVW_{OBJ}^{k} + \Delta VW_{OBJ}^{k+1} \tag{12b}$$

where, $VWIO^{k+1}$ is the net increase in the water volume from the inflow and outflow boundaries and point sources after each time step, $VWIO^{k+1} = \sum_{nb=1}^{NBD} f_{nb} Q_{nb} \cdot \Delta t + \sum_{np=1}^{NPS} q_{np} \cdot \Delta t$, $f_{nb} = 1$ and -1 for inflow and outflow boundaries, respectively. $DVW^{k+1} = VW^{k+1} - VW^{k}$, VW^{k} and VW^{k+1} are the water volume in the model domain at k and $k+1$ time step, respectively.

The model predicted results are presented in Fig. 4. The water storage values predicted by the refined method are very close to the net input water volume values (see Fig. 4a). The accumulated water mass conservation error is also small (see Fig. 4b), with the relative error being about 0.3% in 12 days.where

$$VECIO^{k+1} = \sum_{nb=1}^{NBD} f_{nb} Q_{nb} C_{nb} \cdot \Delta t + \sum_{np=1}^{NPS} q_{np} c_{np} \cdot \Delta t$$

and

$$DVEC^{k+1} = VEC^{k+1} - VEC^{k},$$

VEC^{k} and VEC^{k+1} are the total *E.coli* counts in the model domain at n and n+1 time steps, respectively, in which

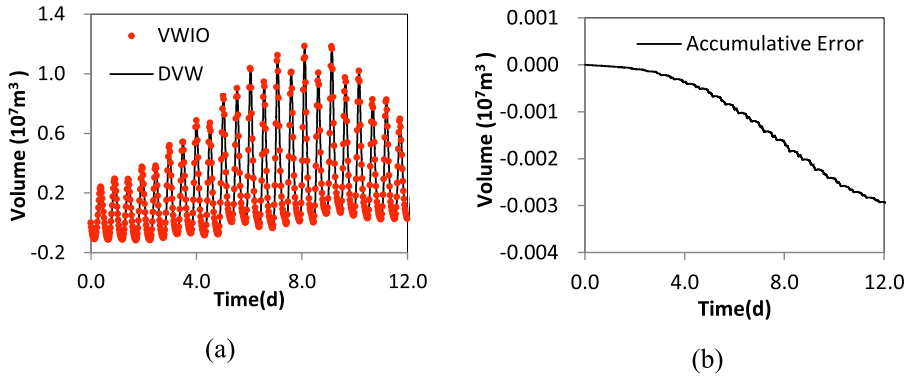

Fig. 4. Conservation analysis of flow mass predictions.

Objective functions similar to Eq. 12 were also used to check the *E.coli* mass conservation levels, as given below.

$$\Delta VEC_{OBJ}^{k+1} = VECIO^{k+1} - DVEC^{k+1} \tag{13a}$$

$$SumVEC_{OBJ}^{k+1} = SumVEC_{OBJ}^{k} + \Delta VEC_{OBJ}^{k+1} \tag{13b}$$

$VEC^{k+1} = \sum_{j=1}^{NSC} A_j^{k+1} \cdot C_j^{k+1} \cdot \Delta X_j$.

For this case, the decay rate for the *E.coli* solution was set to zero. The predicted values of the objective variables are shown in Fig. 5. These results indicate that the level of agreement between *VECIO* and *DVEC* is generally very close (see Fig. 5a). Nevertheless, there is also a relatively small accumulated mass loss (see Fig. 5b), with the average error being around 1.0% of the total *E.coli* number over the simulation period.

3.3. Model verification

In verifying the model the inflow discharges were measured at the 5 main upper boundaries to drive the model. In addition, discharges from the sub-catchments were calculated using the HSPF model, where the calculated discharges were used to compensate for the shortage of measured discharge data in these catchments. Flow discharges and stage data at 3 main control stations (No. 700306, 713056 and 713019, see Fig. 3) were used to verify the enhanced river network model.

It can be seen from Fig. 6a and b that the model predicted and measured flow discharge values at the two control stations (No. 713056 and 713019) in the main channel generally agreed very well for the cases of low and medium flows, with the statistical parameters RMSE, MAE and NSCE being presented in Table 2. The model under-predicted the maximum flood discharges at the two stations on 23rd June 2012, but predicted other peak flows quite well. The errors are thought to be mainly caused by the local rainfall measurements and spatial interpolation errors based on the limited rainfall stations.

The comparison between the predicted water elevations and measured data at stations along the rivers Douglas (No. 700306) and Ribble (No. 713019) respectively agreed satisfactorily (Fig. 6c and d), and the statistical value of the NSCE parameter at these two stations were 0.85 and 0.64 respectively. Other statistics are presented in Table 2. The under-estimated water elevation at flood peak (on 26th September 2012) for the river Douglas (No. 700306) is thought to be caused by the spatial interpolation error of the intense rainfall, based on limited rain gauge stations and flow discharge under estimation by the HSPF model. Further verification will be carried out when new and continuous measured water level data are available.

The *E.coli* concentrations were measured at more than 10 stations in the Ribble catchment by the Centre for Research into Environment and Health (CREH), Aberystwyth University, as a part of the Cloud to Coast (C2C) Project. The results for 2 stations are presented herein (i.e. Fig. 6e and f), with comparisons being given between model predicted and measured *E.coli* concentrations at two sites along the main channel of the river Ribble. It can be seen that the model predicted *E.coli* concentrations generally agree well with the limited measured data, but the model over predicted the concentration during the period from 8th to 28th August 2012. The error analysis results for the parameters RMSE, MAE and NSE are presented and listed in Table 2. The RMSE values are about 1.2 and 0.9 times of the average values of the measurements at these two stations, while the MAE and NSCE values range from 9893.5 cfu/100 ml to 654.9 cfu/100 ml and 0.32 to 0.56 respectively. Since the *E.coli* concentration includes certain uncertainty factors, the predicted *E.coli* concentration values are considered acceptable,

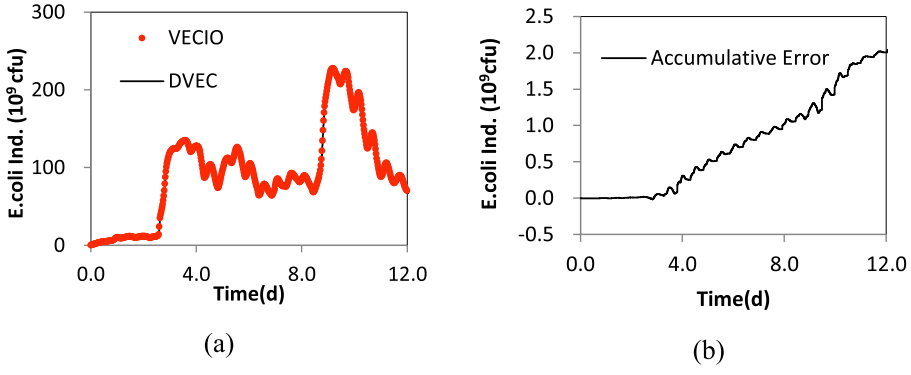

Fig. 5. Conservation analysis of *E.coli* predictions.

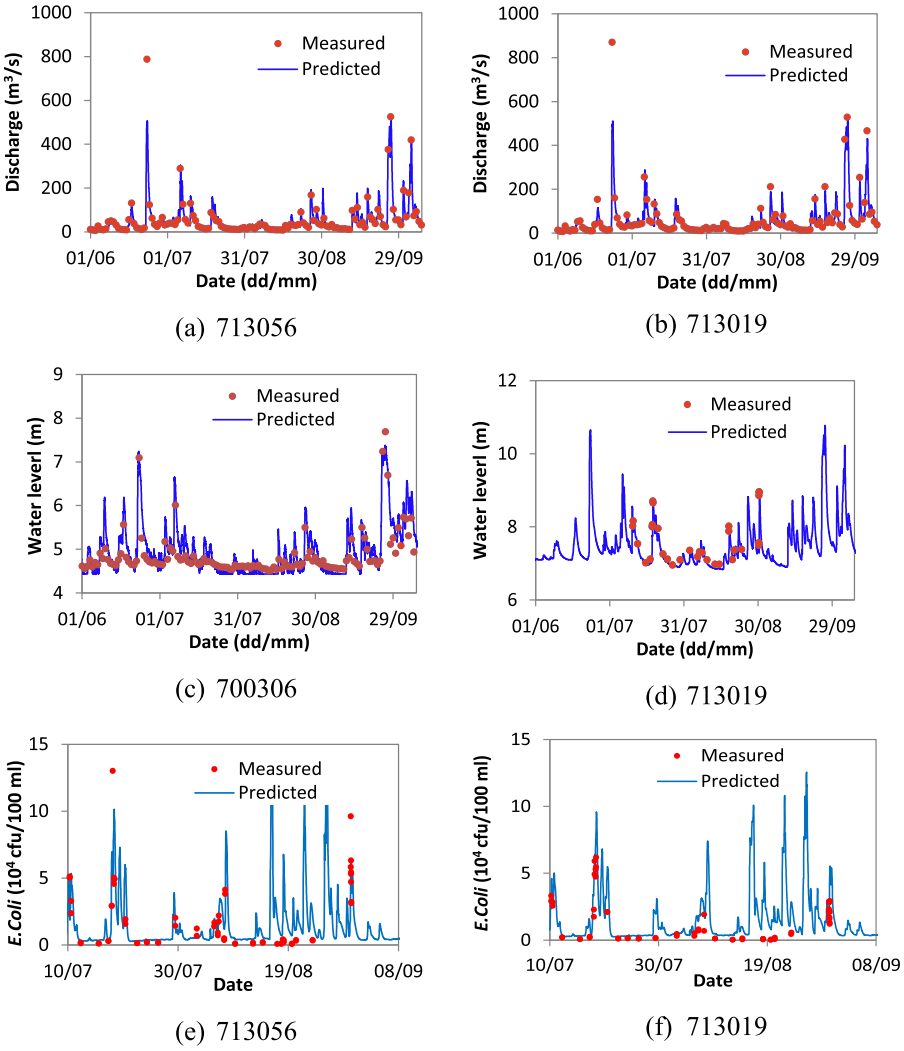

Fig. 6. Verification of discharge, water level and *E.coli* processes.

Table 2
Modelling statistical errors results about the modelling variables at different stations.

Station	Variables	RMSE	MAE	NSCE
No.713056	Q (m3/s)	26.97	4.99	0.85
No.713019	Q (m3/s)	31.93	4.18	0.83
No.700306	Z (m)	0.17	0.05	0.85
No.713019	Z (m)	0.42	0.25	0.64
No.713056	E.coli (cfu/100 ml)	27198.20	−9893.50	0.32
No.713019	E.coli (cfu/100 ml)	12041.30	654.90	0.56

although there are some large errors during the high flow period. The errors in predicting the peak values may be partly attributed to the sparse sampling rate relative to that predicted at each time step in the numerical, and thereby potentially resulting in some high concentration points being missed in the measured data.

3.4. Evolution of stagnation zones in the river Ribble networks

Based on the definition given by Clancy (1975), a stagnation zone is a flow field where the local velocity of the fluid is zero. Stagnation exists extensively at the transition zone between the river and sea, driven mainly by the river flows and tidal currents, and occasionally driven by unsteady flows in the river networks. In the current study the existence of stagnation zones was checked and their dynamic positions were simulated using Eqs. (12) and (13), and the 1-D hydrodynamic model has been extended to include a module on multiple stagnation zones. The generation, movement and extinction of stagnation zones are shown in Fig. 7. Based on the model results, the key processes in the stagnation zones can be summarised as follows: (i) During low ebb phase there is a strong downward flow and thus stagnation does not exist. (ii) During the flood phase, the upward flow from the estuary meets the river flow, then a positive stagnation is generated in the lower estuary (Fig. 7a), it then moves upwards with the tidal currents; with more stagnation zones potentially being formed in river branches of the river network (Fig. 7b). (iii) During the flood to ebb phase, a negative stagnation forms in the lower estuary (Fig. 7c) and it then moves towards the upper reaches, with the previous positive stagnation zones moving downwards. If a sub-channel is long enough, then the positive and negative stagnation zones can coexist (Fig. 7d) until the moving stagnation zones merge and then disappear. Finally, the flow returns to a single downward direction and the processes of phase (i) to (iii) will be repeated. The processes of generation, movement and extinction of the multiple stagnations, driven by the tidal and river flow interactions in the Ribble river networks, were predicted using the numerical model. The results indicate that the multiple stagnation zones may appear in the river networks in the flood to ebb stage.

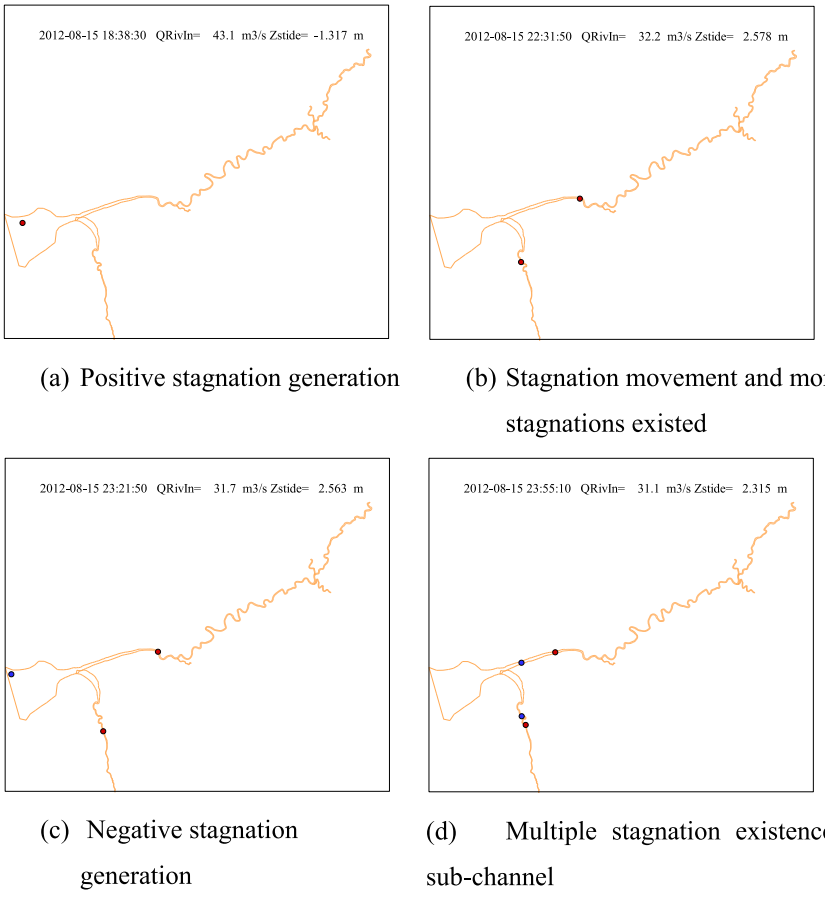

(a) Positive stagnation generation

(b) Stagnation movement and more stagnations existed

(c) Negative stagnation generation

(d) Multiple stagnation existence in a sub-channel

Fig. 7. Model predicted evolution processes of formation and movement of multiple stagnations in Ribble river networks.

Table 3
16 scenarios.

Scenario	Regions	Rural source	Urban source	Note
1	All Ribble	Yes	Yes	Total Ribble region
2	All Ribble	Yes	No	Total Ribble region
3	Upper Ribble	Yes	No	Ribble source to Clitheroe
5	Hodder	Yes	No	Hodder region
5	Calder	Yes	No	Calder region
6	Darwen	Yes	No	Darwen region
7	Douglas	Yes	No	Douglas region
8	Middle Ribble	Yes	No	Clitheroe to Douglas-Ribble junction
9	Lower Ribble	Yes	No	Ribble-Douglas junction to 11 MP
10	Upper Ribble	Yes	Yes	Ribble source to Clitheroe
11	Hodder	Yes	Yes	Hodder region
12	Calder	Yes	Yes	Calder region
13	Darwen	Yes	Yes	Darwen region
14	Douglas	Yes	Yes	Douglas region
15	Middle Ribble	Yes	Yes	Clitheroe to Ribble-Douglas junction
16	Lower Ribble	Yes	Yes	Ribble-Douglas junction to 11 MP

3.5. Source apportionment and its impacts

In order to evaluate the rural and urban source apportionments and its impacts on the lower reach of the river Ribble, 16 one-year scenarios (see Table 3) were simulated, in which the inputs from the 7 sub-catchments were combined (see Fig. 3) to simplify the calculation procedure. The simulation results are shown in Table 4.

It can be seen from Table 4 that in the river Ribble networks the total *E.coli* loss is between 31 and 53%, which varied with different source locations and dynamic weather and hydrodynamic conditions. Before the *E.coli* flux arrives at the tidal limit station (i.e. Bullnose), from the upper reaches, approximately 8% of the *E.coli* died off in the long-narrow middle and upper reaches of the river Ribble. Over 40% of the *E.coli* then died off in the middle and lower reaches. In total, about 80% of the local *E.coli* losses occur in the riverine and estuarine regions from Bullnose to 11 MP for the following reasons: (i) a large retention time caused by the tidal reciprocating flows in the wide and shallow channels; (ii) a higher decay rate due to the increasing salinity levels in the shallow salt marshes (Mancini, 1978), particularly when compared with the fresh water in the upper and middle reaches.

In general, the rural and urban *E.coli* sources have different characteristics. The rural region, with a large proportion of *E.coli* sources from livestock, is generally located in the upper and middle reaches of the river basin, while the urbanised communities with an important portion of *E.coli* from domestic sewage, industrial waste water etc. are located in the lower reaches of the river basin, close to the receiving waters, i.e. estuaries and coastal zones. The urban *E.coli* sources are controlled more frequently by man-made devices, such as Waste water treatment plants (WWTPs) and Combined sewer Overflows (CSOs), with the retention and transportation times for *E.coli* general being increased and decreased respectively in these devices. Thus, they may cause a non-consistent phase difference between the flow discharge and the *E.coli* fluxes. The transport time and related loss rate for urban source usually varies considerably, especially for extreme flow events. The general transport time for rural *E.coli* sources can therefore be shorter than the corresponding urban sources, although the distance between the rural *E.coli* source and the receiving waters is usually longer. In the Ribble river networks, the overall *E.coli* decay rate from the rural source is about 3% higher than that from urban sources.

Table 4
Model predicted *E.coli* loss (%) in the model domain (From 30th June to 31st September 2012).

IID	Region	Rural				Rural + Urban			
		Bullnose	3 MP	7 MP	11 MP	Bullnose	3 MP	7 MP	11 MP
1	Up Ribble	8.24	9.01	19.10	52.37	8.21	9.03	19.11	52.16
2	Hodder	8.19	8.67	17.19	52.77	8.19	8.69	17.30	52.88
3	Calder	4.28	4.47	11.98	39.32	3.98	4.41	10.51	41.30
4	Darwen	1.00	3.83	6.51	34.53	1.85	5.33	11.26	46.90
5	Douglas			9.62	32.38			10.61	42.05
6	Mid Ribble		8.54	16.92	45.84		2.00	15.86	48.71
7	Low Ribble				35.11				31.19
8	Total Ribble	7.03	8.28	17.61	49.44	6.09	8.07	16.52	

Meanwhile, there is some exceptional variations in the Darwen sub-catchment where the urban *E.coli* source is dominant, due to the highly urbanised level and population density in the basin.

4. Discussion

4.1. Validity and effectiveness of the proposed methods

The accuracy of the solution of the 1-D mass transport equation depends partly on the representation of the hydrodynamic equations and partly on the accuracy of the discretization method of these equations. Moreover, the errors from the hydrodynamic solutions may be transferred to the mass transport solutions and may even cause fluctuations in the solutions. The 1-D St. Venant equations with z and Q being main variables frequently used in the engineering community are not strictly conservative (Cunge et al., 1980) because of the approximation ($\frac{\partial A}{\partial t} = B\frac{\partial Z}{\partial t}$), and the error from the approximation during linearization will increase when the width B varies significantly within a time step in a river, particularly where a shallow and wide river has a narrow deep main channel. In order to enhance a consistent solution between the hydrodynamic and mass transport equations, limited inner iterations in Eq. (1) are carried out to reduce the error from the flow solution.

The Preissmann scheme is based on a bi-diagonal implicit finite difference method for solving the 1-D St. Venant equations and is unconditionally stable and robust. However, the mass and momentum equations, i.e. Eqs. (1) and (2), are only equivalent to the discretized equation (Appendix S1: Eqs. (2) and (3)) when the conditions $\Delta A << A$ and $\Delta Q << Q$ are satisfied. For some special conditions, e.g. near bank-full discharge, low tide or stagnant flows, ΔA or ΔQ may be of a similar order of magnitude, or even larger, than A and Q, then the assumed conditions cannot be satisfied and some large errors may occur in the hydrodynamic solutions. In order to enhance the Preissmann scheme, the method of limited inner iterations with a smaller time step is used (Hu et al., 2010), together with the mass conservation check in the hydrodynamic solutions. Also, the transformation from the finite difference method (FDM) to FVM based on the staggered variables distribution improves the mass conservation level of the solution. Furthermore, the solution for multiple stagnation zones makes the model predictions closer to the real physical process for tidal wave propagation and the interaction with the flow in river networks.

4.2. E.coli concentration difference at stations

In order to evaluate the model results, a comparison was made of the predictions (Fig. 8) made using the three methods, including: (i) the finite difference method, (ii) the finite volume method with a single stagnation zone (FVM_S), and (iii) the finite volume method with multiple stagnation zones (FVM_M) at 2 stations (No. 9 MP and No. DGS995) in Fig. 3. During the calculation, the main parameters such as decay rate, and returning coefficient (=0.1) were kept the same. The main findings can be summarised as follows: (i) in the upper and middle reaches, the *E.coli* concentration differences between the FDM and FVM algorithms is small because the flow direction is identical; (ii) in the lower region, because of the existence of a reversing current, the mass loss is relatively large when the FDM algorithm is used, and there is a relatively large *E.coli* concentration difference between the FDM and FVM algorithms at the 9 MP station (Fig. 8a and b) and DGS_995 station (Fig. 8c and d); and (iii) there may be more than one stagnation zone in a sub-channel driven by the tidal and river flows, especially during the second-half of the spring to ebb tidal period. Since the duration of multiple stagnation zones in the Ribble river is relatively short, the impact of multiple stagnation zones is minor on the *E.coli* processes and the predicted concentration difference between a single and multiple stagnation zones is small in the main river and the estuarine region. However, in the river Douglas, the occurrence of multiple stagnation zones is more common because of the weak river flow, the strong tidal currents and the long branched channel with a small bed slope. Therefore, in this river, the predicted difference in the *E.coli* concentrations between the two FVM methods is much larger than that in the river Ribble (Fig. 8d). The refinement of the solution method makes the predictions closer to the physical process and increases the model's generality when compared to the original method. Moreover, the solution is more stable when the FVM algorithm is used.

4.3. E.coli loss rate (%) by different methods

It can be seen from Table 4 that the FDM_S algorithm can predict larger *E.coli* losses due to its non-conservation property, and the FVM algorithm can enhance the mass conservation level by up to 10%, with the same decay rate and returning coefficients at the lower boundary. There are no obvious difference in the *E.coli* predictions with single and multiple stagnations zones when the two FVM algorithms are compared, as confirmed by the percentage losses shown in Fig. 8 and Table 5. The decay rate in lower river reaches and the estuarine waters is larger than that in the upper riverine reaches and about 16–48% of the *E.coli* will die-off in the lower river reaches and the estuarine waters. Meanwhile, because of heterogeneity in the bed sediments and vegetation in the region, the transport processes and the fate of *E.coli* in the lower river reaches and the estuary are complex and further study is needed in order to reduce the level of uncertainty.

5. Conclusions

A refined one-dimensional model has been developed for improving the mass-conservation solution properties for solute mass fluxes, particularly for *E.coli*, using consistent equations, a staggered grid and transformation from a FDM to a FVM algorithm. Moreover, an enhanced approach is proposed to solve the mass transport equation in a sub-channel where there may be multiple stagnation zones, which may be a general phenomenon in the lower reaches of a tidal river. The test case for the Ribble river basin and estuary shows that the mass-conservation level reaches 99.0% after 12 days of simulation using the

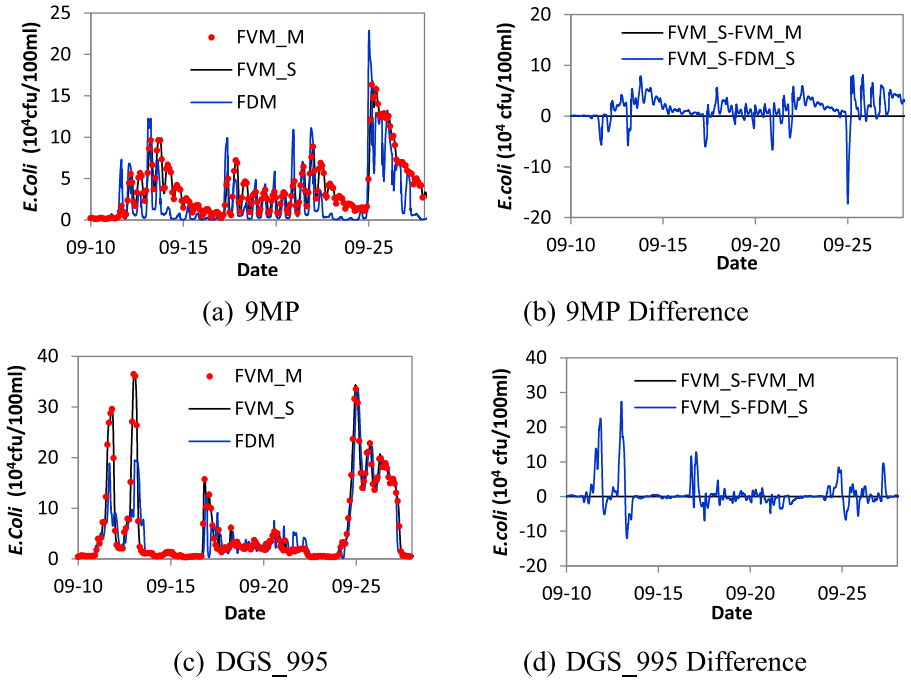

Fig. 8. Comparison of the *E.coli* concentration processes predicted using the FDM_S, FVM_S and FVM_M algorithms.

Table 5
E.*coli* loss (%) at different positions using FDM_S, FVM_S and FVM_M.

Method	Region	Rural + Urban			
		Bullnose	3 MP	7 MP	11 MP
FDM_S	Rib	7.97	9.21	25.10	56.27
FVM_S_1It	Rib	6.09	8.55	17.29	48.10
FVM_S_2It	Rib	5.17	8.55	16.54	47.27
FVM_S_3It	Rib	5.21	8.74	16.02	46.75
FVM_S_5It	Rib	5.76	8.58	15.86	46.67
FVM_M	Rib	6.09	8.52	16.52	45.38

Note: It = inner iteration.

refined model and for an extremely complex flow and tidal dynamics scenario, with the model generally predicting: the discharge, water elevations and *E.coli* concentrations to a high degree of accuracy for the highly unsteady field measurements acquired in 2012. The refined and verified 1-D model has been applied to 16 one-year scenarios for different *E.coli* source apportionments based on the results obtained using the HSPF and Infoworks models. The results from these model scenarios indicate the following:

(i) The degree of mass conservation in the numerical model solution is a prerequisite condition for the evaluation of the source, transport and fate of *E.coli* bacteria.
(ii) In the Ribble catchment, the *E.coli* inputs are mainly from the Darwen, Calder, and Douglas rivers, and the middle and lower reaches of the river Ribble, with highly urbanised and high population density areas contributing a large proportion of these inputs. The transport time and related loss rate for the urban sources usually varies considerably. Typically 16–48% of the *E.coli* died off during the transport processes from the input sources to the river Ribble outlet, with these findings being attributed to the complex hydrodynamic and tidal conditions predicted in the modelling system.
(iii) The fate of *E.coli* concentrations was found to be closely linked to the source positions, and the solute and mass transport processes associated with the local hydrodynamic and salinity conditions.

Acknowledgements

The research reported herein was funded by the Natural Environment Research Council, the Medical Research Council, the Department for Environment, Food and Rural Affairs and the Economic and Social Research Council, GR NE/I008306/1, UK. The authors are also grateful to the Environment Agency North West for their provision of data and to all colleagues from the universities of Aberystwyth and Sheffield working on the NERC C2C project and, in particular, to Professor David Kay and Dr Carl Stapleton of the Centre for Research into Environment and Health (CREH), who provided the concentration data for source apportionment. The detailed and rigorous comments made by the three anonymous reviewers are also much appreciated.

Appendix A. Supplementary data

Supplementary data related to this article can be found at https://doi.org/10.1016/j.envsoft.2018.07.009.

References

Aral, M.M., Zhang, Y., Jin, S., 2000. Closure to "application of relaxation scheme to wave-propagation simulation in open-channel networks" by Mustafa M. Aral, Yi Zhang, and Shi Jin. J. Hydraul. Eng. 126 (1) 91–91.
Bicknell, B., Imhoff, J., Kittle, J., Donigian, A., Johanson, R., 1997. Hydrological Simulation Program — FORTRAN: User's Manual for Version 11.
Bladé, E., Gómez-Valentín, M., Dolz, J., Aragón-Hernández, J.L., Corestein, G., Sánchez-Juny, M., 2012. Integration of 1D and 2D finite volume schemes for computations of water flow in natural channels. Adv. Water Resour. 42 (0), 17–29. https://doi.org/10.1016/j.advwatres.2012.03.021.
Bousso, S., Daynou, M., Fuamba, M., 2012. Numerical modeling of mixed flows in storm water systems: critical review of literature. J. Hydraul. Eng. 139 (4), 385–396. https://doi.org/10.1061/(ASCE)HY.1943-7900.0000680.
Clancy, L.J., 1975. Aerodynamics. Halsted Press, Pitman, London.
Cunge, J.A., Holly, F.M., Verwey, A., 1980. Practical Aspects of Computational River Hydraulics. Pitman Publishing Ltd., London.
Delis, A., Skeels, C., Ryrie, S., 2000. Implicit high-resolution methods for modelling one-dimensional open channel flow. J. Hydraul. Res. 38 (5), 369–382. https://doi.org/10.1080/00221680009498318.
Falconer, R.A., 1984. Temperature distributions in tidal flow field. J. Environ. Eng. 110 (6), 1099–1116.
Fischer, H.B., 1973. Longitudinal dispersion and turbulent mixing in open-channel flow. Annu. Rev. Fluid Mech. 5 (4), 59–78.
Hu, J., Li, S., Geng, B., Long, W., 2010. Correction of the problem of non-conservation of

mass existing in the one-dimensional scalar transport model for river-networks. Chinese Journal of Hydrodynamics 25 (3), 337–343. https://doi.org/10.3969/j.issn.1000-4874.2010.03.009.
Huang, G., Falconer, R.A., Lin, B., 2017. Integrated hydro-bacterial modelling for predicting bathing water quality. Estuar. Coast Shelf Sci. 145–155.
Huang, G., Lin, B., Zhou, J., Chen, Q., Falconer, R., 2014. A new spatial interpolation method based on cross-sections sampling. In: International Conference on Hydroinformatics, City College of New York, pp. 1–7.
Jin, M., Coran, S., Cook, J., 2002. New one-dimensional implicit numerical dynamic sewer and storm model. In: Proc. 9th Int. Conf. Urban Drainage–global Solutions for Urban Drainage, pp. 1–9.
Kay, D., Wyer, M., Crowther, J., Stapleton, C., Bradford, M., McDonald, A., Greaves, J., Francis, C., Watkins, J., 2005. Predicting faecal indicator fluxes using digital land use data in the UK's sentinel Water Framework Directive catchment: the Ribble study. Water Res. 39 (16), 3967–3981. https://doi.org/10.1016/j.watres.2005.07.006.
Lauer, J.W., Viparelli, E., Piégay, H., 2016. Morphodynamics and sediment tracers in 1-D (MAST-1D): 1-D sediment transport that includes exchange with an off-channel sediment reservoir. Adv. Water Resour. 93, 135–149. https://doi.org/10.1016/j.advwatres.2016.01.012.
Mancini, J.L., 1978. Numerical estimates of coliform mortality rates under various conditions. Journal 2477–2484.
Merkhali, S.P., Ehteshami, M., Sadrnejad, S.A., 2015. Assessment quality of a nonuniform suspended sediment transport model under unsteady flow condition (case study: aras River). Water Environ. J. 10. https://doi.org/10.1111/wej.12137.
Murillo, J., Navas-Montilla, A., 2016. A comprehensive explanation and exercise of the source terms in hyperbolic systems using Roe type solutions. Application to the 1D-2D shallow water equations. Adv. Water Resour. 98, 70–96. https://doi.org/10.1016/j.advwatres.2016.10.019.
Nanía, L.S., León, A.S., García, M.H., 2014. Hydrologic-hydraulic model for simulating dual drainage and flooding in urban areas: application to a catchment in the metropolitan area of chicago. J. Hydrol. Eng. 20 (5), 1–13. https://doi.org/10.1061/(ASCE)HE.1943-5584.0001080.
Paiva, R.C.D., Collischonn, W., Tucci, C.E.M., 2011. Large scale hydrologic and hydrodynamic modeling using limited data and a GIS based approach. J. Hydrol. 406 (3–4), 170–181. https://doi.org/10.1016/j.jhydrol.2011.06.007.
Salvadore, E., Bronders, J., Batelaan, O., 2015. Hydrological modelling of urbanized catchments: a review and future directions. J. Hydrol. 529, 62–81. https://doi.org/10.1016/j.jhydrol.2015.06.028.
Sanders, B.F., Green, C.L., Chu, A.K., Grant, S.B., 2001. Case study: modeling tidal transport of urban runoff in channels using the finite-volume method. J. Hydraul. Eng. 127 (10), 795–804.
Servais, P., Garcia-Armisen, T., George, I., Billen, G., 2007. Fecal bacteria in the rivers of the Seine drainage network (France): sources, fate and modelling. Sci. Total Environ. 375 (1–3), 152–167. https://doi.org/10.1016/j.scitotenv.2006.12.010.
Steets, B.M., Holden, P.A., 2003. A mechanistic model of runoff-associated fecal coliform fate and transport through a coastal lagoon. Water Res. 37 (3), 589–608. https://doi.org/10.1016/S0043-1354(02)00312-3.
Stelling, G.S., 2003. A staggered conservative scheme for every Froude number in rapidly varied shallow water flows. Int. J. Numer. Meth. Fluid. 43 (12), 1329–1354. https://doi.org/10.1002/d.537.
Twigt, D.J., Goede, E.D.D., Zijl, F., Schwanenberg, D., Chiu, A.Y.W., 2009. Coupled 1D–3D hydrodynamic modelling, with application to the pearl river delta. Ocean Dynam. 59 (6), 1077–1093. https://doi.org/10.1007/s10236-009-0229-y.
Wallingford Software Ltd, 1995. In: HydroWorks On-line Documentation Wallingford,HR, UK, Ltd, W.S.
Wu, W., Vieira, D.A., Wang, S.S., 2004. One-dimensional numerical model for nonuniform sediment transport under unsteady flows in channel networks. J. Hydraul. Eng. 130 (9), 914–923.
Wu, W., Wang, S.S., 2008. One-dimensional explicit finite-volume model for sediment transport. J. Hydraul. Res. 46 (1), 87–98. https://doi.org/10.1080/00221686.2008.9521846.
Yang, L., Lin, B., Falconer, R.A., 2008. Modelling enteric bacteria level in coastal and estuarine waters. Proc. ICE - Eng. Comput. Mech. 161 (4), 179–186.
Zhang, S., Duan, J.G., Strelkoff, T.S., Bautista, E., 2011. Simulation of unsteady flow and soil erosion in irrigation furrows. J. Irrigat. Drain. Eng. 138 (4), 294–303. https://doi.org/10.1061/(ASCE)IR.1943-4774.0000396.
Zhang, W., Lyu, S., Zhu, Y., Chen, X., 2014. A coupled model of the 1d river network and 3D estuary based on hydrodynamics and suspended sediment simulation. Journal of Applied Mathematics 2014 14. https://doi.org/10.1155/2014/798579.
Zhou, J., Lin, B., 1998. One-dimensional mathematical model for suspended sediment by lateral integration. J. Hydraul. Eng. 124 (7), 712–717.